Mapping the Binding Interface of the Cytochrome b_5−Cytochrome *c* Complex by Nuclear Magnetic Resonance†

Weiping Shao,‡,§,|| Sang-Choul Im,‡ Erik R. P. Zuiderweg,*,§ and Lucy Waskell*,‡

Department of Anesthesiology, University of Michigan, VA Medical Center, 2215 Fuller Road, Ann Arbor, Michigan 48105, and Biophysics Research Division, University of Michigan, 930 North University Avenue, Ann Arbor, Michigan 48109

Received June 9, 2003; Revised Manuscript Received October 3, 2003

ABSTRACT: The interaction between bovine cytochrome b_5 (cyt b_5) and horse heart cytochrome *c* (cyt *c*) is investigated by NMR spectroscopy. Chemical shifts of cyt b_5 backbone resonances and side chain methyl resonances were monitored as a function of cyt *c* concentration. The shifts are small but saturatable and indicate that the binding of cyt b_5 with cyt *c* is in fast exchange. An equilibrium association constant of $(6 \pm 3) \times 10^4$ M^{-1} was obtained with a lower limit of 180 s^{-1} for the dissociation rate of the complex. To resolve considerable ambiguities in the interpretation of the chemical shift mapping, ^{15}N relaxation experiments and cross-saturation experiments were used as alternative methods to map the cyt b_5−cyt *c* binding interface. Results from the three experiments combined demonstrate that the conserved negatively charged region of cyt b_5 surrounding the solvent-exposed heme edge is involved in the interaction with cyt *c*. These data support the models proposed by Salemme and Mauk [(1976) *J. Mol. Biol. 102,* 563−568; (1993) *Biochemistry 32,* 6613−6623].

Cytochrome b_5 (cyt b_5)[1] has been implicated in several key electron transfer processes with a variety of redox partners. Perhaps the most extensively studied electron transfer complex is that between ferrocytochrome b_5 and ferrocytochrome *c* (cyt *c*). Spectroscopic measurements have established that these proteins form a complex with a 1:1 stoichiometry (*1*). An exception to this generalization is the complex between rabbit cyt b_5 and yeast iso-1 cyt *c*. At high molar ratios, a weak ternary complex of one molecule of cyt b_5 and two molecules of cyt *c* has been shown to exist (*2*). Another study in which the adequacy of controls has been questioned also suggests a ternary complex may occur at high cyt *c*:cyt b_5 ratios (*3*, *4*). The strong pH and ionic strength dependence of this protein−protein association suggests that electrostatic interactions are important for the formation of the electron transfer complex. The crystal structures of cyt b_5 and cyt *c* reveal that the heme groups in both proteins are surrounded by a conserved set of charged amino acids (Figure 1) (*4*). The surface at the predicted interface of cyt b_5 is composed of a conserved negatively charged region, while cyt *c* has a number of conserved lysine residues that complement the cyt b_5 interface (*5*, *6*). On the basis of these data, several models of the cyt b_5−cyt *c* complex have been developed. Docking the static structures,

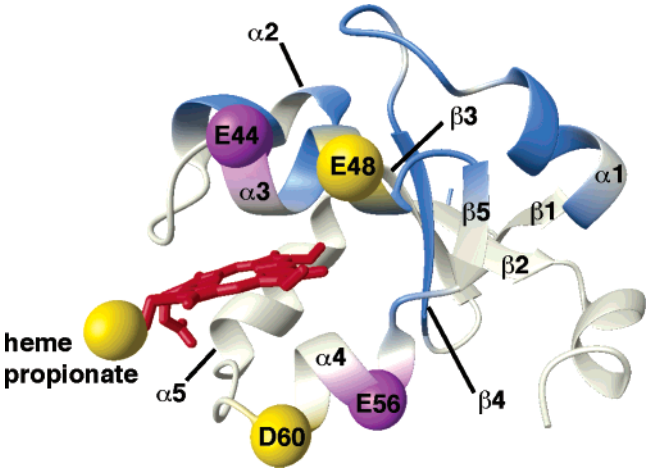

FIGURE 1: Ribbon representation of the crystal structure of bovine cyt b_5 (PDB entry 1cyo) (*57*). The conserved negatively charged residues that are believed to be important in the cyt *c*−cyt b_5 interaction are depicted and labeled (*5*−*7*). The gold residues represent amino acids common to both the Salemme and Mauk models. Glu44 is represented in the Salemme model and the less stable complex form in the Mauk study. Glu56 is represented only in the most stable complex identified by Brownian dynamics (*7*). The ribbon is colored blue to designate the region containing the mobile loop, which has been proposed to form a cleft to serve as an alternate binding site for cyt *c*. (*9*). The heme is colored red. The figure was made using MOLMOL (*34*).

Salemme proposed a model of the complex dominated by the complementarily charged side chains that surround the exposed hemes in both proteins. In this model, the solvent-exposed hemes of the two proteins are approximately 8 Å apart in an orientation only 15° from coplanar (*5*, *6*). Further modeling studies of the tuna cyt *c*−bovine cyt b_5 complex using molecular dynamics simulations resulted in a configuration of the complex that is more favorable for electron

† Supported by a Veterans Administration Merit Review, NIH Grant GM3533 to L.W., and NIH Grant GM52421 to E.R.P.Z.

* To whom correspondence should be addressed E-mail: zuiderwe@umich.edu or waskell@umich.edu.

‡ Department of Anesthesiology, University of Michigan, VA Medical Center.

§ Biophysics Research Division, University of Michigan.

|| Current address: Molecular Staging Inc., 300 George St., New Haven, CT 06511.

[1] Abbreviations: NMR, nuclear magnetic resonance; HSQC, heteronuclear single-quantum coherence; cyt b_5, soluble domain of cytochrome b_5; cyt *c*, cytochrome *c*.

10.1021/bi030145t CCC: $25.00
Published on Web 11/21/2003

transfer with a reduced Fe−Fe distance. Brownian dynamics calculations on a model complex between yeast cyt *c* and bovine cyt b_5 yielded two stable complexes with binding interfaces that also involved the surfaces containing the exposed hemes (*7*). One of the complexes between yeast cyt *c* and bovine cyt b_5 incorporated a set of salt bridges similar to that of the Salemme model (Figure 1). Significantly more stable was a slightly translated complex which was dominated by an alternate set of salt bridges between the proteins. Site-directed mutagenesis and hyperbaric pressure spectroscopy were used to map the interface between the interaction domain of microsomal cyt b_5 and mitochondrial cyt *c* (*8*). These studies showed the area surrounding the exposed heme edge in cyt b_5 is involved in the protein−protein interface and suggest that several intermolecular electrostatic interactions are important for complex stability.

Daggett and co-workers have identified a loop in cyt b_5 (Glu10−Ser20) on an alternate face of the molecule that exhibits conformational mobility in molecular dynamics calculations (Figure 1) (*9*). In a departure from the electrostatically dominated interaction, they have calculated that cyt *c* can form a stable complex by binding to amino acids exposed when the cleft on cyt b_5 is open (*10*). Their studies raise the possibility that movement of the loop renders a previously buried hydrophobic region accessible for binding to cyt *c*.

There has been limited success using crystallography to study electron transfer complexes of moderate affinity that are dominated by electrostatic contacts. Therefore, the structural characterization of the cyt b_5−cyt *c* complex and other electron transfer complexes has been performed largely by NMR spectroscopy (*3*, *10*−*15*). Mapping the perturbation of chemical shifts upon complex formation provides a highly sensitive tool for identifying the residues that play a role in the interaction (*11*, *16*, *18*−*21*). Previous NMR studies of the cyt b_5−cyt *c* complex have monitored the chemical shift changes of resolved hyperfine-shifted proton resonances of paramagnetic components. However, perturbations to heme resonances caused by complex formation could not provide high-resolution information about the location of the binding site because the pseudocontact effect induced by the anisotropic paramagnetic center of components was observed for protons as far as 20 Å from the heme (*17*). Selective ^{13}C labeling of the ϵ-carbon of the lysine residues in cyt *c* or heme propionates in cyt b_5 was used to locate the binding interface between the two proteins (*14*, *15*).

In a previous NMR study, the backbone chemical shifts of labeled ferrous cyt b_5 in the absence and presence of unlabeled ferrous cyt *c* were compared (*10*). Two regions in cyt b_5 exhibited chemical shift differences upon complex formation. One region consisted of the anionic surface surrounding the heme, and the other was consistent with molecular dynamics studies which identified an alternate binding cleft that is formed upon movement of the loop region containing residues Glu10−Ser20. These chemical shift mapping studies created some ambiguity with respect to the location of the binding interface on cyt b_5.

In the current work, the NMR studies have been extended by monitoring a full titration series of ^{15}N- and ^{13}C-labeled ferrous cyt b_5 with unlabeled ferrous cyt *c*. To obtain a more complete picture of the interaction, we monitored chemical shift changes in not only the backbone but also the side chain methyl groups. From these data, the association constant and the lower limit of k_{off} could be calculated. The chemical shift changes induced in the cyt b_5 molecule upon titration with cyt *c* were mapped on the structure to identify the residues affected by complex formation. Since the chemical shift changes were unable to unambiguously delineate the interface, ^{15}N relaxation experiments were performed to characterize changes in the dynamic behavior of cyt b_5 upon complex formation with cyt *c*. In addition, a cross-saturation experiment was carried out to better define the intermolecular interface. From the combined experiments, it was possible to conclude that the interaction interface is consistent with both of the slightly different models first proposed by Salemme (*5*, *6*) and Mauk and co-workers (*7*). The results presented here do not support the earlier report which suggested an alternative binding site (*10*).

MATERIALS AND METHODS

Sample Preparation. Cyt b_5 was expressed and purified as previously described (*10*). Briefly, the synthetic cyt b_5 gene that includes the DNA sequence encoding the water-soluble domain (Ala3−Arg84, Asn17Asp) of bovine liver cyt b_5 was cloned into the T7 expression vector, pHB40P. The resulting plasmid, pHBb5, was used to transform *Escherichia coli* strain BL21(DE3) and or strain BL21(DE3)-pLysS for the generation of unlabeled and ^{15}N- and ^{13}C-labeled proteins, respectively. For ^{15}N-, ^{13}C-, and ^{2}H- and ^{15}N-labeled cyt b_5, the 1 L cultures were grown in media containing 600 mL of ^{15}N- and ^{13}C-labeled Celtone media (Martek), ^{13}C-labeled sodium acetate (2 g/L), or ^{2}H- and ^{15}N-labeled Celtone media (Martek), $FeCl_3$ (1 mM), $ZnSO_4$ (15 mM), $MnCl_2$ (3.9 mg/mL), $MgSO_4 \cdot 7H_2O$ (10 mg/mL), K_2HPO_4 (18 mg/mL), KH_2PO_4 (14 mg/mL), NaCl (17 mM), thiamine (5 mg/mL), and a vitamin mixture (biotin, choline chloride, folic acid, niacinamide, D-pantothanate, pyridoxal, and riboflavin, each at 2.5 mg/mL). Expression was induced by addition of IPTG to a final concentration of 0.5 mM. Twelve hours after induction, the cells were separated from the supernatant by centrifugation. Most of the cyt b_5 was found in the supernatant where it was present as the apoprotein. The holoprotein was reconstituted from apo-cyt b_5 by addition of 1 mM hemin (in basic 50% ethanol) to the supernatant, which was then dialyzed against 50 mM potassium phosphate buffer (pH 7.2). Anion exchange chromatography using DE-52 resin (Whatman) was followed by gel filtration chromatography using a column of Sephadex G-75 (Pharmacia). Fractions with an A_{413}/A_{280} ratio of >5.9 were pooled and concentrated. The protein purity was determined by SDS−PAGE analysis and mass spectrometry. The final yield was 100 mg/L of uniformly ^{15}N- and ^{13}C-labeled cyt b_5 with ^{15}N and ^{13}C isotope enrichment of 99% according to MALDI mass spectroscopy.

To express the [^{2}H,^{15}N]cyt b_5, C41 cells (Avidis, Saint Beauzire, France) were grown in increasing concentrations of D_2O (10, 30, 60, 80, and 100%). A single colony was grown in 10 mL of a 100% D_2O/LB medium/0.24 mM carbenicillin mixture with shaking at 250 rpm and 37 °C to an A_{600} of 0.8−1.0 (∼24 h). The cells were pelleted and resuspended in 5 mL of a fresh 100% D_2O/LB medium/0.24 mM carbenicillin mixture; 250 μL of these cells were added to 100 mL of a 100% D_2O/[^{2}H,^{15}N]Celtone medium/0.24 mM carbenicillin mixture in a 1 L Erlenmeyer flask. The cells

were grown at 25 °C with shaking at 250 rpm. When the OD at 600 nm was 1.2−1.5 (∼35 h), IPTG was added to a final concentration of 0.5 mM. The culture was incubated for an additional 24 h at 25 °C with shaking at 250 rpm. The cells were pelleted and disrupted by sonication with care to prevent the temperature from increasing above 12 °C. A 1.2-fold molar excess of hemin was added to reconstitute the expressed apocyt b_5 which was then purified as described in the previous paragraph.

Horse heart cyt *c* (type VI) was purchased from Sigma and used without further purification.

The ^{15}N- and ^{13}C-labeled cyt b_5 and unlabeled cyt *c* were buffer exchanged under nitrogen pressure into 1 mM potassium phosphate buffer at pH 7.0 (YM3 membranes, Amicon). The sample volumes were reduced to make concentrated stock solutions. Protein concentrations were determined spectrophotometrically utilizing an $\epsilon_{412.5}$ of 117 mM^{-1} cm^{-1} for ferricyt b_5 (*22*) and an $\epsilon_{409.5}$ of 106 mM^{-1} cm^{-1} for ferricyt *c* (*23*).

Ten individual samples for the titration of ferrous (reduced) cyt b_5 with ferrous cyt *c* were prepared under anaerobic conditions in a glovebox equipped with a BASF catalyst column for the removal of oxygen. All solutions, including 1 mM potassium phosphate buffer (pH 7.0), the KOH solution (for adjusting pH), standard pH solutions, and H_2O, were purged with nitrogen to minimize the introduction of oxygen into the glovebox. These solutions, together with cyt b_5 and cyt *c* stock solutions, pH meter, pipets, and NMR tubes, were equilibrated overnight in the glovebox. The concentration of cyt b_5 was kept constant, and cyt *c* was added to obtain the desired the cyt *c*:cyt b_5 molar ratios. The concentration of cyt b_5 in each sample was 0.8 mM with the concentration of cyt *c* varying from 0 to 2.4 mM to yield samples containing cyt *c*:cyt b_5 molar ratios of 0.15, 0.3, 0.6, 0.9, 1.6, 2.0, 2.5, and 3.0. The samples were then reduced by addition of a 50 or 100% molar excess of a freshly made sodium dithionite solution. The concentration of the sodium dithionite was calibrated by titration with riboflavin under anaerobic conditions. As the addition of sodium dithionite decreased the pH of the samples, the pH was adjusted to 7.0 (±0.02) with KOH inside the glovebox. The samples were then sealed using a torch under slight N_2 overpressure.

NMR Experiments. The NMR titration and relaxation experiments were carried out at 25 °C on a Bruker AMX500 or DRX500 spectrometer equipped with a triple-resonance probe with a *Z*- or *X*-, *Y*-, and *Z*-pulsed field gradient, respectively.

^{1}H−^{15}N fast-WATERGATE-HSQC spectra (*24*) of ^{15}N- and ^{13}C-labeled ferrous cyt b_5 unbound and in a complex with cyt *c* at different cyt *c*:cyt b_5 ratios were recorded with spectral widths of 7692 Hz for ^{1}H and 1773 Hz for ^{15}N as an array of 4K × 200 complex points. ^{1}H−^{13}C CT-HSQC spectra for doubly ^{13}C- and ^{15}N-labeled ferrous cyt b_5 alone and in complex (cyt *c*:cyt b_5 ratio of 2.0) were collected with spectral widths of 8333.3 Hz and 4K complex points in the ^{1}H dimension and 10 000.0 Hz and 480 complex points in the ^{13}C dimension (*25*).

Transverse ^{15}N relaxation rate (R_2) experiments were carried out using a two-dimensional ^{1}H-detected heteronuclear pulse sequence without suppression of chemical/conformational exchange broadening (*26*−*28*). The R_2 relaxation period contained a single ^{15}N 180° pulse, while scalar coupling and cross-correlation effects between ^{1}H and ^{15}N in this period were suppressed by a ^{1}H composite-pulse decoupling sequence. All spectra were acquired with a spectral width identical to that used in the titration experiments using 4096 complex points in the ^{1}H dimension and 256 complex points in the ^{15}N dimension. R_2 values were obtained from eight experiments with relaxation delays of 10, 20, 30, 50, 70, 90, 110, and 118 ms for cyt b_5 alone and 10, 20, 30, 40, 50, 70, 84, and 98 ms for the cyt b_5−cyt *c* complex.

The cross-saturation experiments were performed on samples containing 0.8 mM ferrous [^{2}H,^{15}N]cyt b_5 in 1 mM potassium phosphate (pH 7.0) in a 1:1 H_2O/D_2O mixture alone or with 0.96 mM cyt *c* on a Varian Inova spectrometer at 18.1 T (800 MHz for ^{1}H) as described by Shimada and co-workers (*29*). To maximize the magnetization transfer, the temperature was reduced to 15 °C. The saturation was achieved with an adiabatic decoupling sequence (*30*) using a bandwidth of 3.75 ppm centered at 1.8 ppm to cover the lysine side chains as well as aliphatic protons. Control experiments were carried out to ascertain that the H_2O resonance was not affected by the saturation field. Off-resonance experiments were carried out with the center of the decoupling field shifted 20 000 Hz upfield. Because the heme present in cyt b_5 is protonated and can therefore provide a significant background, a set of on-resonance/off-resonance experiments was also performed with cyt b_5 alone. Any residues that exhibited decreases in peak height upon application of the saturation in the free cyt b_5 were disregarded in the analysis of cross-saturation data for the complex.

All of the NMR spectra were processed using NMRPipe (*31*) and analyzed with NMRView (*32*) or XEASY (*33*) software. In general, the time domain data were zero-filled in the indirect dimensions and apodized with shifted sine bell or Lorentzian-to-Gaussian window functions. Linear prediction was applied to indirect heteronuclear dimensions acquired with constant-time evolution. Molecular representations were made with the program MOLMOL (*34*).

Analysis of Chemical Shift Changes. Chemical shifts of the cyt b_5 in the complex with cyt *c* were compared with the resonance assignments of cyt b_5 alone. Normalized weighted average chemical shift differences Δav (=$\Delta\delta/\Delta\delta_{max}$) for cyt b_5 amide ^{1}H and ^{15}N chemical shifts upon cyt *c* binding were calculated using the equation $\Delta\delta(NH) = \{[\Delta\delta H^2 + (\Delta\delta N/5)^2]/2\}^{1/2}$ (*5*, *8*), where $\Delta\delta$H and $\Delta\delta$N are the differences in chemical shift observed between the bound and free states. The corresponding weighted averages for the side chain methyl groups were calculated using the equation $\Delta\delta(CH) = \{[\Delta\delta H^2 + (\Delta\delta C/4)^2]/2\}^{1/2}$, where $\Delta\delta$H and $\Delta\delta$C are the chemical shift differences observed for the methyl protons and carbons, respectively, between the bound and free states (*16*). The normalized weighted average chemical shift differences were mapped onto the structure of cyt b_5.

Calculation of Ring Current Shifts. Ring current shifts were calculated using a program from M. Williamson at University of Sheffield (Sheffield, England) (*35*), which uses the Haigh−Mallion method (*36*) with ring current intensity factors taken from Ösapay and Case (*37*). The X-ray structure of cyt b_5 (PDB entry 3b5c) was used for calculating the ring current shifts of each amide proton of cyt b_5.

RESULTS AND DISCUSSION

Confirmation of the Resonance Assignments for Cyt b_5. Previous NMR experiments have established that two forms of cyt b_5 exist in solution due to a 180° rotation of the heme about the α,γ-meso axis (*38*). For bovine cyt b_5, the ratio between the states is 9:1; it is only the most populated state that is addressed in this paper. The sequential backbone resonance assignments were confirmed using a pair of experiments (HNCA and HNCOCA). Side chain assignments were confirmed from three-dimensional (3D) HCCH-TOCSY and 3D ^{15}N-resolved NOESY-HSQC spectra. The amide proton for Gly41, which lies directly over the heme ring, was shifted extremely upfield and assigned to the position of 1.07 and 129 ppm ($^1H^N$ and ^{15}N, respectively). The assignments that were obtained are in good agreement with those reported previously (*10*, *12*, *39*).

Titration of Cyt b_5 with Cyt c. Two-dimensional ^{1}H−^{15}N HSQC NMR spectra were used to monitor the titration of ^{15}N- and ^{13}C-labeled cyt b_5 with unlabeled cyt *c*. Chemical shift perturbations and increases in line width were observed in the spectrum of cyt b_5 upon formation of the complex with cyt *c*. A superimposition of the HSQC spectra of free cyt b_5 and that in the complex with cyt *c* (cyt *c*:cyt b_5 ratio of 2.0) is depicted in Figure 2A. The line width of the ^{1}H−^{15}N cross-peaks increased over the range of the titration in a saturatable manner (Figure 3A), providing strong evidence of a stable intermolecular interaction. The chemical shift changes observed upon complex formation were relatively small in magnitude and involved only a subset of the cyt b_5 resonances (Figure 2). Although small, the chemical shift changes can be interpreted with confidence, because the pH and ionic strength were painstakingly controlled over the titration (see Materials and Methods). One of the more significant changes in the ^{1}H−^{15}N HSQC spectra over the titration with cyt *c* involves ^{N}Hδ of the Asn57 side chain. The intensity of the cross-peaks corresponding to the two protons of the ^{δ}NH$_2$ group increases during the titration with cyt *c*, while in the spectrum of free cyt b_5, the corresponding resonances are almost completely broadened away by chemical or conformational exchange. This observation suggests either a reduction in the rotation about the $C_γ$−$N_δ$ bond or a decrease in the rate at which the ^{N}Hδ protons exchange with water upon binding cyt *c* (Figure 2A, inset).

The changes in the amide proton chemical shifts and signal intensities of cyt b_5 at molar ratios of cyt *c* ranging from 0 to 3.0 are shown in Figure 3. The binding constant, K_a, was determined from the data using eq 1:

$$\Delta Y = \frac{\Delta Y_\infty}{2}(A - \sqrt{A^2 - 4R}) \quad (1)$$

where

$$A = 1 + R + \frac{BR + C}{B}CK_a \quad (2)$$

in which R is the molar ratio of cyt *c* to cyt b_5, ΔY is either the intensity change (Figure 3A) or chemical shift change (Figure 3B,C), ΔY_∞ is the estimated peak intensity or chemical shift for the state where $R \rightarrow \infty$, and B and C are the total cyt b_5 and cyt *c* concentrations, respectively (*40*). K_a is the equilibrium association constant assuming a bimolecular interaction. The fit yields a K_a of $(6 \pm 3) \times 10^4$ M^{-1} at 1 mM potassium phosphate buffer at pH 7.0 and 25 °C. The uncertainty represents the reproducibility of fitting the ^{1}H and ^{15}N chemical shift changes for four different residues (His26, Gly51, Val61, and His63) and variation in the peak intensities for the same peaks over the titration. The calculated binding constant agrees well with the K_a of $(3.8 \pm 1.4) \times 10^4$ M^{-1} measured for the formation of the soluble mitochondrial membrane ferricyt b_5−ferricyt *c* complex at an ionic strength (*I*) of 20 mM at 30 °C (*14*). Others have reported values of $(8 \pm 3) \times 10^4$ M^{-1} at pH 7.0 and an *I* of 10 mM (*1*) and 960 ± 100 M^{-1} at an *I* of 40 mM (*41*) for the formation of the complex between cyt b_5 and cyt *c*. The range of values for the affinity constants found in the literature can be attributed to the varying species involved in the complexes and the differences in conditions under which the measurements were taken. In particular, the interaction between the two cytochromes is strongly dependent on ionic strength. However, assessing the ionic strength for solutions containing the high concentrations of charged proteins required for these experiments in the presence of low salt concentrations is difficult.

A single resonance peak is observed for each amide of cyt b_5 at any point during the titration. Therefore, the cyt b_5−cyt *c* complex is in fast exchange on the NMR time scale between its unbound and bound forms. Line broadening due to exchange processes was not observed. A maximum chemical shift change of 29 Hz for the amide proton of His63 provides a lower limit for the dissociation rate (k_{off}) of 180 s^{-1} ($k_{off} \gg 2\pi\Delta\delta$, where $\Delta\delta$ is the maximum observed difference in chemical shift between the free and complexed form of cyt b_5). A lower dissociation rate would cause line broadening which is not observed in this study.

Ring Current Shift Calculations. Chemical shift perturbations that accompany the binding of two proteins are often interpreted to map to the binding interface. However, as chemical shifts report only on the local magnetic shielding environment of the nuclei, using backbone chemical shift changes to identify protein residues that are involved in specific intermolecular interactions must be interpreted with care. In the case of cyt b_5 and similar proteins containing a diamagnetic heme, amino acid residues close to the heme are subject to large ring current effects (*42*). Therefore, a small perturbation of the relative heme orientation due to complex formation could give rise to sizable proton chemical shift changes remote from the binding interface. To assess these effects, the theoretical changes in the ring current shifts that would be induced by a 0.1 Å movement of the heme in any direction were calculated for all amide protons in cyt b_5. The ring current shifts were assessed at every position in the protein for a heme movement of this magnitude in any of six directions ($-x$, $+x$, $-y$, $+y$, $-z$, and $+z$). In this way, a measure of the derivative of the ring current shift with respect to spatial movement of the heme was obtained. These theoretical ring current shift derivatives calculated for cyt b_5 are compared with the differences in amide proton chemical shifts that occur upon cyt *c* binding in Figure 4. The largest ring current shift derivative among the amide protons of cyt b_5 was calculated for the Gly41 amide proton. This was expected, since this proton experiences the largest ring current effect in the protein to start (it resonates at 1.03 ppm) and should thus be the most sensitive sensor for

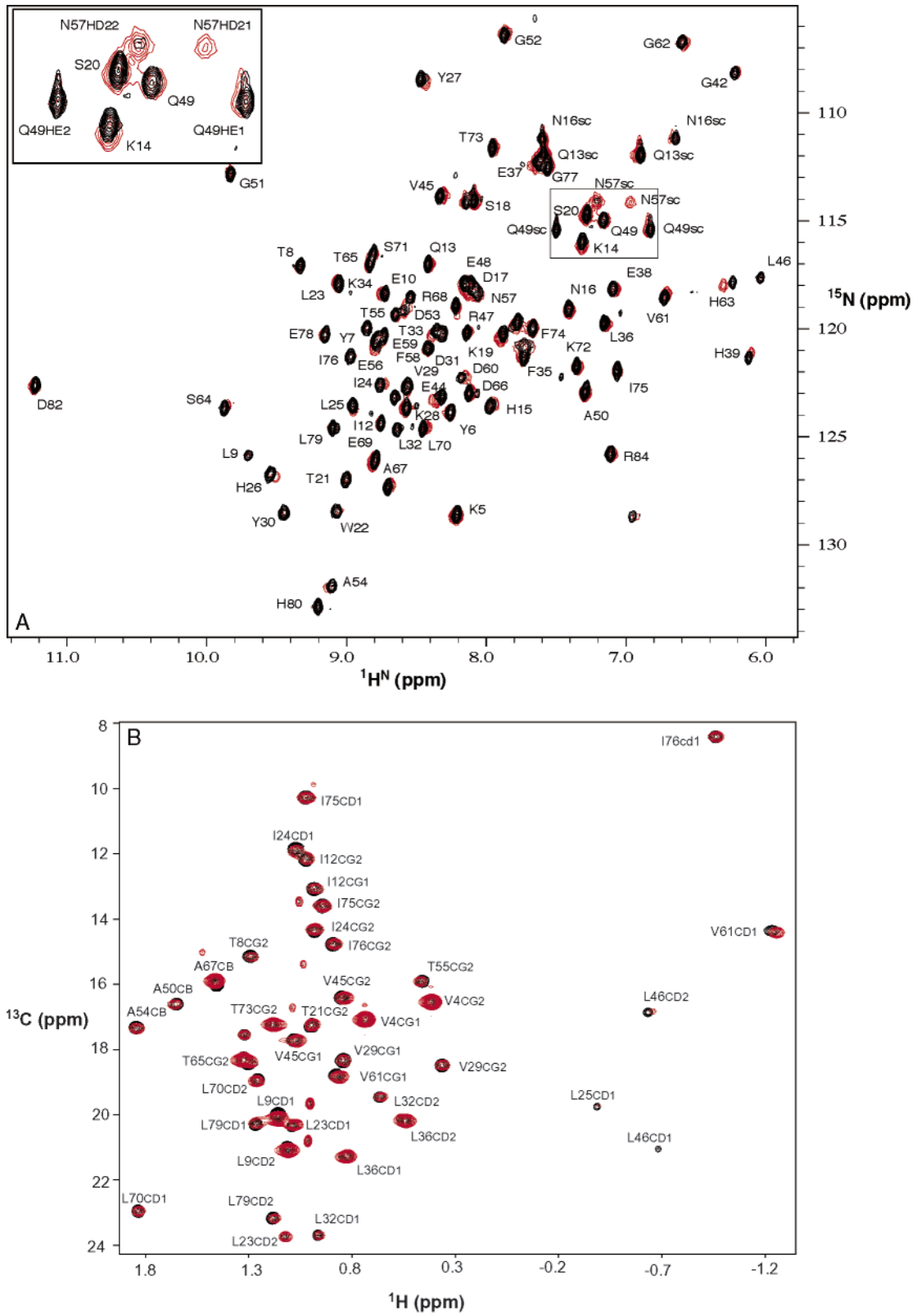

FIGURE 2: Superposition of the amide region of the $^{1}H-^{15}N$ HSQC spectra (A) and the methyl group region of the $^{1}H-^{13}C$ HSQC spectra (B) of free ^{15}N- and ^{13}C-labeled ferrous cyt b_5 (black) and ^{15}N- and ^{13}C-labeled ferrous cyt b_5 in the complex (red) with unlabeled ferrous cyt *c* in a cyt *c*:cyt b_5 ratio of 2.0. The cross-peaks are labeled with sequence specific assignments. In the inset of panel A is shown a comparison of the cross-peaks corresponding to the $^{N}H\delta$ protons of the Asn57 side chain.

changes in the heme position. We compute that a hypothetical 0.1 Å heme movement would cause a 0.125 ppm chemical shift change for this proton. Since the observed chemical shift change for this residue was only 0.02 ppm, we may infer that adjustments to the cyt b_5 heme position are at most a few hundredths of an angstrom, and that ring current effects can consequently be neglected as a major source of shifts for most residues. Moreover, for many other residues for which experimental chemical shift perturbations were observed, no ring current effects were predicted at all for 0.1

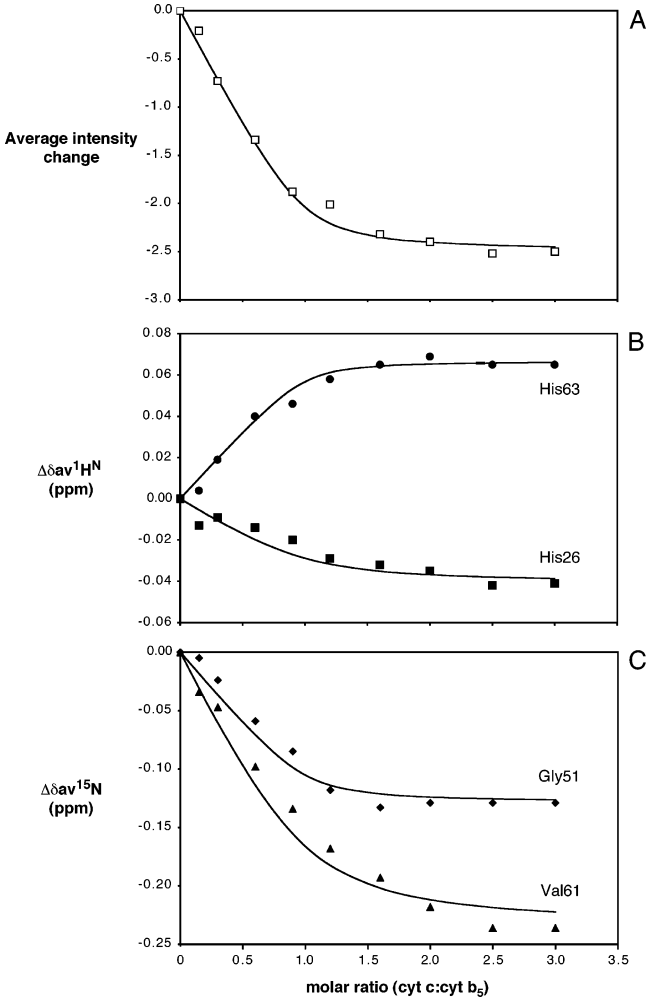

FIGURE 3: Titration of cyt b_5 with cyt *c*. (A) Changes in peak intensity are plotted as a function of the molar ratio of cyt *c* to cyt b_5. (B) Amide proton ($^1H^N$) chemical shift changes of residues His63 and His26. (C) Amide nitrogen (^{15}N) chemical shift changes of residues Gly51 and Val61. The curves represent the best fits of the individual data using eq 1 defined in the text.

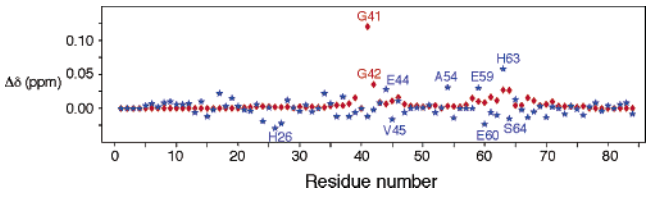

FIGURE 4: Comparison of predicted ring current shift changes for the amide protons after a 0.1 Å change in the position of the heme with the experimentally observed chemical shift changes (blue) for the amide proton resonances of cyt b_5 due to the binding of cyt *c*. The ring current shift effects were calculated by averaging the ring current chemical shift changes caused by the 0.1 Å movement of heme relative to the rest of the molecule in three-dimensional space (red) (see the text for more details). The amide proton chemical shift changes represent differences observed between the free cyt b_5 and the cyt b_5 in complex with cyt *c* (cyt *c*:cyt b_5 ratio of 2.0) (blue).

Å movements. Thus, with the possible exception of those residues in the immediate vicinity of the heme, our analysis strongly suggests that the chemical shift perturbations observed upon cyt *c* binding are not due to changing ring current shifts, but to other sources of magnetic perturbation, such as intermolecular contact and/or conformational change.

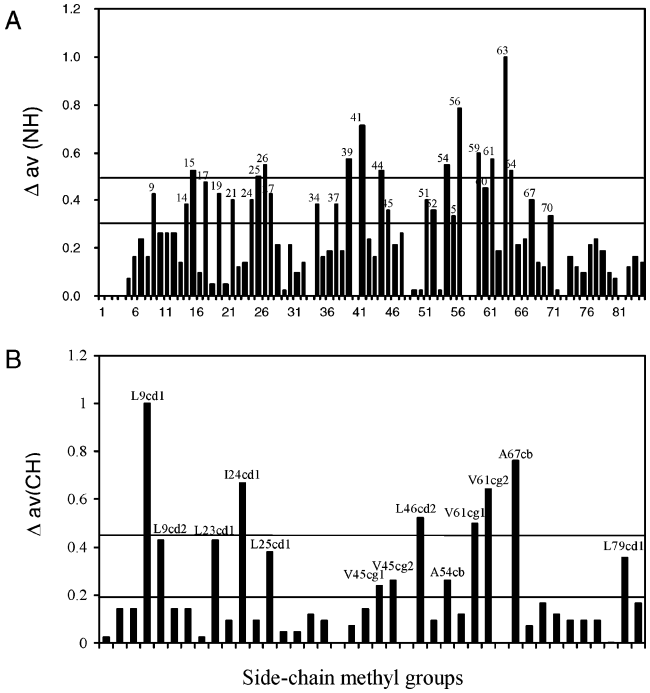

FIGURE 5: Normalized weighted average of chemical shift differences (Δav) for backbone amide (A) and side chain methyl groups (B) of cyt b_5 upon complexation with cyt *c*. The bottom line represents the mean chemical shift change, and the top line signifies the mean value plus one standard deviation. Normalized weighted average chemical shift differences Δav ($=\Delta\delta/\Delta\delta_{max}$) for cyt b_5 amide ^1H and ^{15}N chemical shifts upon cyt *c* binding were calculated using the equation $\Delta\delta(NH) = \{[\Delta\delta H^2 + (\Delta\delta N/5)^2]/2\}^{1/2}$, where $\Delta\delta H$ and $\Delta\delta N$ are the differences in chemical shift observed between the bound and free states. The weighted average shifts for cyt b_5 methyl ^1H and ^{13}C chemical shifts differences were calculated using the equation $\Delta\delta(CH) = \{[\Delta\delta H^2 + (\Delta\delta C/4)^2]/2\}^{1/2}$, where $\Delta\delta H$ and $\Delta\delta C$ are the chemical shift differences observed for the methyl protons and carbons, respectively, between the bound and free states.

The saturation transfer experiments described below help distinguish these cases.

Chemical Shift Changes Observed upon Binding of Cyt c. The chemical shift changes induced in cyt b_5 by cyt *c* binding were mapped using the normalized weighted average chemical shift differences of the backbone amide ^1H and ^{15}N resonances, Δav(NH) (Figure 5). There are several possible reasons for the small magnitude of the observed chemical shift changes. The low affinity of the cyt b_5−cyt *c* complex may be capable of causing only small perturbations in local structure and would hence cause only small chemical shift changes. Electrostatic forces are believed to be important for the recognition and preorientation of the two proteins, suggesting a model of the binding interface involving primarily interactions between charged side chains. As the chemical shift mapping experiments are not optimal for detecting these types of interactions, this could explain the small absolute value of the observed chemical shift changes. As a result of studies on formation of the complex of cyt b_5 and myoglobin, a model of an electron transfer complex that is dynamic in nature has been proposed (*43*, *44*). In this model of recognition, the cluster of complementarily charged residues in each of the proteins initiates the interaction. Once the interaction is established, a small translation or rotation is proposed to optimize the complex for electron transfer. Thus, there may be an ensemble of analogous complexes.

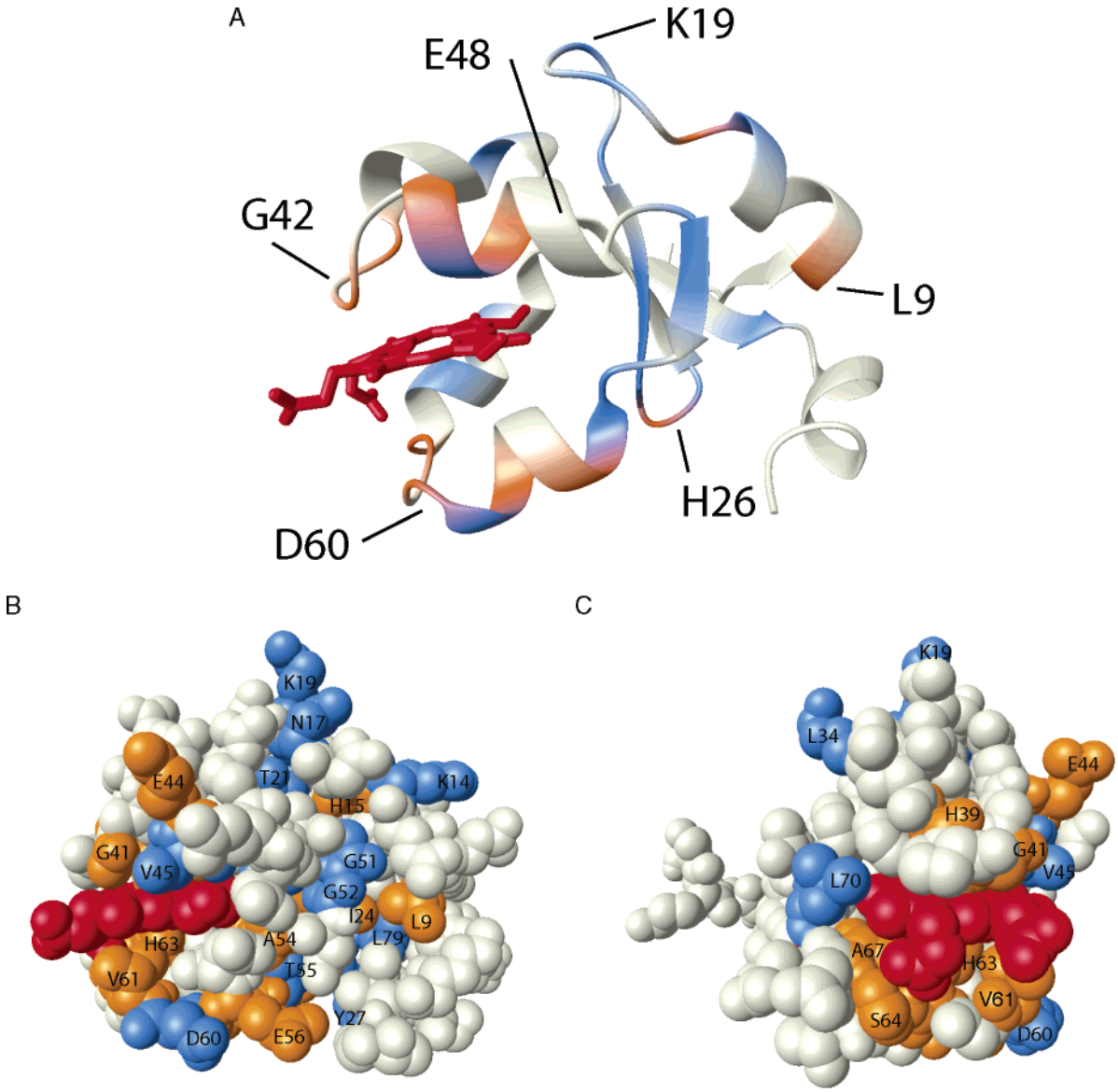

FIGURE 6: Chemical shift mapping of cyt *c* binding with cyt b_5. (A) Ribbon representation of cyt b_5 (PDB entry 1cyo) (*57*). The residues colored orange represent those that exhibited a normalized weighted average of chemical shift difference (Δav) of amide and methyl groups greater than the mean value plus one standard deviation. Residues with Δav values between the mean value and the mean plus one standard deviation are colored blue. The heme is colored red. (B) Same as panel A, but shown on a space filling model of cyt b_5. (C) A 90° rotation of panel B. This figure was made using MOLMOL (*34*).

A "rolling ball" model of the complex between cyt b_5 and cyt *c* in which movement occurs about specific regions of the interface has been suggested previously (*45*). In addition, a nonrigid model complex has been proposed for the electron transfer complex of plastocyanin with cytochrome *f* (*46*). If such a mobile model applies to the cyt *c*−cyt b_5 complex, the observed spectra could represent the average of several nonidentical complexes utilizing largely overlapping interfaces. A group of structurally similar complexes could be the source of the small magnitude of the observed chemical shift changes.

Two clusters of residues with significantly shifted resonances can be distinguished (Figure 5). The larger group of residues is located in the region surrounding the surface-exposed heme, corresponding to the "Salemme" site (Figures 5 and 6). The residues exhibiting the largest changes include the axial ligands His39 and His63, Gly41 which is located in the loop connecting helices α2 and α3, Glu44 in helix α3, Ala54, Glu56, Glu59, and Val61 in helix α4, and Ser64 in the loop linking helices α4 and α5. Helices α2−α5 form much of the heme binding pocket (Figure 1). The other group of chemical shift changes is localized in another region of the molecule, and includes His15 in helix α1, Leu25 at the end of the *β*-strand *β*4, and His26 in the loop region that connects strands *β*4 and *β*3. The latter site involves several residues corresponding to the "cleft" area identified previously (*9*, *10*) (Figure 6).

As side chains commonly play a dominant role in molecular recognition, we have investigated the chemical shift changes for the side chain methyl groups of cyt b_5 upon complexation with cyt *c*. The $^{1}H-^{13}C$ HSQC spectrum of cyt b_5 overlaid on that of the cyt b_5−cyt *c* complex is depicted in Figure 2B. Perturbations are small here as well and are observed primarily in the same two regions observed with the backbone chemical shift mapping (Figures 5 and 6). Again, a concentration of chemical shift changes is

located in the region of the solvent-exposed heme. The side chain methyl groups of Val45γ1, Val45γ2, and Leu46δ2 which are located in helix α3 and Ala54β, Val61γ1, and Val61γ2 of helix α4 all exhibit changes in chemical shift upon binding of cyt *c*. Changes are also observed in the second "cleft" region, and are represented by chemical shift changes for the methyl groups of Leu9δ1 which is located in helix α1 and Leu23δ1, Ile24δ1, and Leu25δ1 of strand β3.

While both of these regions correspond with the locations of clusters of chemical shift changes observed in the same system in a previous study (*10*), the distribution and exact residues that experience a change in the local chemical environment are significantly different. In the earlier study, the majority of the changes occurred around the region containing the mobile loop (cleft) region (Glu10−Ser20) while the perturbations at the face of cyt b_5 containing the exposed heme (Salemme site) were limited. In contrast, this study shows a larger number of chemical shift changes in the Salemme site (indicated in orange in Figure 6). The differences between these studies may possibly be attributed to the way the samples were prepared. Our study establishes that the chemical shift variations as a function of cyt *c* concentration in both regions of cyt b_5 occurred concurrently throughout the titration. These data strongly suggest that there is only a single binding site for horse heart cyt *c* on bovine cyt b_5. The diffusion coefficient of the complex has established that it is a 1:1 complex (*10*), and NMR spin relaxation data of the complex (see below) are also consistent with a 1:1 complex. The chemical shift mapping results cannot establish whether the binding site is an extended area including mostly the Salemme and partially the cleft area, or a more restricted interaction at the Salemme site, causing subtle long-range conformational changes and/or altered charge effects at the cleft site. Consequently, chemical shift mapping alone is found to be insufficient for the delineation of the details of the cyt *c* binding site.

In contrast to our results with bovine cyt b_5 and horse heart cyt *c*, it has been observed that rabbit cyt b_5 has two binding sites for yeast iso-1-cyt *c* and that in the presence of excess cyt *c* a 1:2 cyt b_5−cyt *c* complex is formed (*2*). Thus, the experimental results vary depending on the source of the cyt b_5 and cyt *c* proteins (*47*). Experiments that purported to demonstrate a ternary complex with one molecule of cyt b_5 and two molecules of cyt *c* are considered experimentally flawed (*4*).

Measurement of the Backbone ^{15}N Relaxation Rates (R_2). Mapping changes in local dynamic behavior has also been utilized to identify binding interfaces as changes in the dynamic behavior of residues in the binding site often accompany ligand recognition (*48*−*51*). To this end, ^{15}N R_2 relaxation rates of cyt b_5 were measured in the presence and absence of cyt *c*.

The salient effect is a 2.7-fold increase in the R_2 relaxation rate upon complexation. This increase exceeds the increase in molecular weight upon complexation which is consistent with the formation of a nonglobular complex of two globular proteins (i.e., correlation time and R_2 are proportional to the molecular weight for globular molecules only). The second effect of complexation is that the R_2 relaxation rates in the complex become more monotonic than in the free protein. That is, residues Tyr27, Glu38, Ala54, Val61, Gly62, and

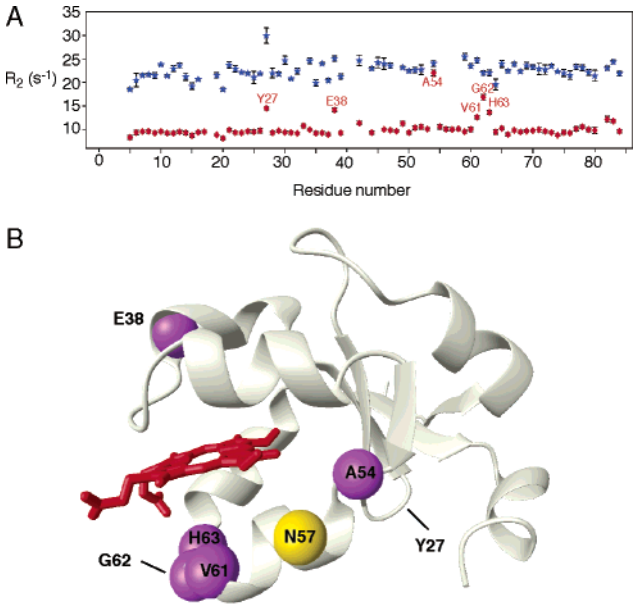

FIGURE 7: Binding surface of cyt b_5 as defined by ^{15}N relaxation rate (R_2) measurements. (A) Comparison of backbone ^{15}N relaxation rates (R_2) in free cyt b_5 (red) and the complex with cyt *c* (blue). Conformational exchange broadening was minimally suppressed with the sequence that was used (see the text). (B) The changes in relaxation rate (conformational exchange) upon complexation with cyt *c* are mapped onto a ribbon representation of bovine cyt b_5. The residues exhibiting a significant change in relaxation rate relative to that of the rest of the molecule are shown in purple (Glu38, Ala54, Val61, Gly62, and His63). Also exhibiting a change in dynamics upon binding to cyt *c* is Asn57, which is colored gold (see the inset of Figure 2A). The heme is colored red (PDB entry 1cyo) (*57*). This figure was made using MOLMOL (*34*).

His63 in the free cyt b_5 exhibit a higher transverse relaxation rate (R_2) than the rest of the molecule (Figure 7A). The increased relative rate for these residues can be attributed to conformational fluctuations on the milli- to microsecond time scale, as the relaxation difference could be suppressed by using a Carr−Purcell−Meiboom−Gill (CPMG) pulse sequence (data not shown) (*27*, *28*). Upon formation of a complex with cyt *c* (cyt *c*:cyt b_5 ratio of 2.0), residues Glu38, Ala54, Val61, Gly62, and His63 located near the heme of cyt b_5 exhibit an ^{15}N relaxation rate similar to that of the rest of the protein (Figure 7B). Thus, it appears that the millisecond conformational fluctuations of these residues of cyt b_5 were quenched by the binding of cyt *c*. Milli- to microsecond motions have often been observed by NMR spectroscopy for apoprotein surfaces that are destined to be interfaces in complexes (*48*). The increased level of motion is likely an indication of the adaptability of the interfacial residues for an induced-fit optimization in the complex. The quenching of the millisecond dynamics by cyt *c* for several residues at the heme area of cyt b_5 therefore suggests that this region is the primary binding site.

The relaxation data are consistent with the participation of the highly conserved cluster of negatively charged residues, i.e., Glu44, Glu48, Glu56, and Asp60, and heme propionate in the binding interface with cyt *c*, i.e., the Salemme site. As discussed earlier, a change in the dynamic behavior was also observed for the Asn57 side chain during the titration with cyt *c*. Since the Asn57 side chain is surface-exposed in the uncomplexed protein, the observed change in the dynamic behavior suggests that this area participates

in the protein−protein interface between cyt b_5 and cyt *c*. The alternate cleft region identified in the chemical shift mapping is comprised of residues Leu9, Lys14, His15, Asn17, Lys19, Leu23−Tyr27, Lys34, Glu37, and Leu46, where His15 exhibits one of the largest observed amide backbone chemical shift changes. While one residue in this region, Tyr27, exhibits conformational flexibility that is different from that of the rest of cyt b_5, the dynamic behavior of this residue remains unchanged upon complexation with cyt *c*, which suggests that this region is not involved in the cyt *c* binding interface.

Cross Saturation of the Cyt b_5−Cyt c Complex. Cross-saturation techniques can provide more direct evidence of the binding interface between two proteins through magnetization transfer from the aliphatic protons of one protein to the amide protons of a second ^{2}H- and ^{15}N-labeled protein. In this system, the magnetization of the aliphatic protons of unlabeled cyt *c* is saturated. It then diffuses through the binding interface to the amide protons of the ^{2}H- and ^{15}N-labeled cyt b_5 whose amide protons had been back exchanged in H_2O. The cross saturation causes a decrease in the peak height of the resonances of the amide protons that are spatially close to the binding interface. The experiment was optimized for this system by using a broad saturation to cover not only the aliphatic protons of the cyt *c* but also the protons in the lysine side chains which have previously been implicated as important participants in the recognition process (*5*−*7*, *15*). To lower the protein rotational correlation time and thus enhance the saturation transfer rate, the sample temperature was lowered from 25 to 15 °C.

Several resonances exhibited a decrease in peak height, which is indicative of participation in the protein−protein interface. A significant loss in peak height was defined as more than one standard deviation from the average change in peak height upon application of the saturation. Several residues surrounding the protonated heme exhibited decreases in peak height for cyt b_5 alone (Val29, Tyr30, Val45, Glu56, Asn57, Ser64, Ser71, and Ile76). These residues were disregarded in the analysis of the data for the complex. In general, the decreases in peak height for the complex were smaller in magnitude than those reported for other complexes (*29*, *52*, *53*). As previously discussed, this could be due to the fact that the complex is dominated by electrostatic interactions that are not optimal for this type of analysis, due to the fact that a high background due to the shifted amide proton of Gly41, or perhaps a result of the two proteins sampling multiple relative orientations, a trait that has been proposed to be characteristic of electron transfer complexes (*13*, *43*, *46*). The resonance corresponding to Gly42 exhibits the greatest decrease in intensity (∼30%). Other residues that appear to be on the interface include Glu43, Leu46, Glu59, and Asp60. Gly42 and Glu43 lie in the loop that connects helices α2 and α3, which itself contains Leu46. Glu59 and Asp60 are located in helix α4 on the opposite side of the heme. The residues that are affected lie primarily on the surface of cyt b_5 surrounding the exposed heme (Figure 8), which is the region predicted to be at the protein−protein interface by the models of Salemme and Mauk (*5*−*7*). Gly77, which lies on the opposite side of the protein, also exhibits a decrease in peak height. We cannot provide an explanation for this effect, but note that the neighboring residue Ile76 also exhibits a decrease in peak height in the control

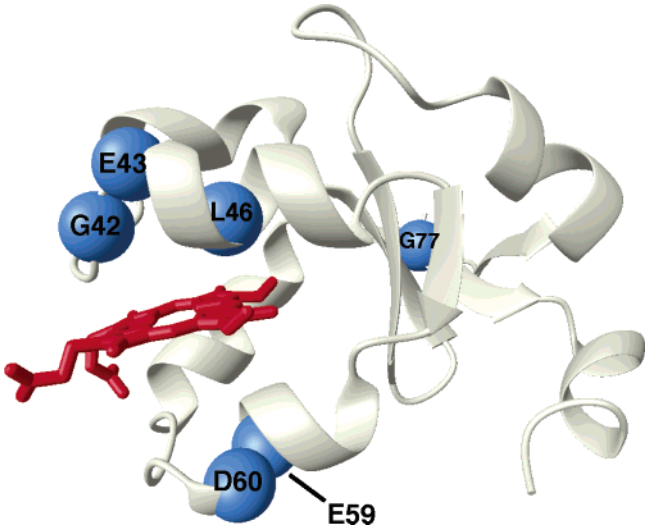

FIGURE 8: Residues identified by a cross-saturation experiment to be involved in the cyt *c*−cyt b_5 binding interface. Residues that exhibit decreases in peak intensity that are greater than one standard deviation from the average change that occurs upon applying the saturation are colored blue. The heme is colored red (PDB entry 1cyo) (*57*). This figure was made using MOLMOL (*34*).

experiment. Thus, with the exception of this residue, the cross-saturation data are consistent with the relaxation data and comprise the subset of the residues identified by the chemical shift mapping that correspond to the model of the cyt b_5−cyt *c* complex proposed by Salemme and Mauk (*5*−*7*). Conspicuously absent in the collection of residues in the binding interface with cyt *c* according to the cross-saturation experiment are those that are suggestive of an alternate binding site (Glu10−Ser20, Leu23−Tyr27, Lys34, Glu37, and Leu46) (*10*).

The combined data consisting of chemical shift mapping, exchange broadening quenching, and cross saturation are summarized in Figure 9, and provide strong evidence of the exclusive binding of cyt *c* to the cyt b_5 site proposed by Salemme and Mauk (*5*−*7*). Models of cyt b_5 in complex with metmyoglobin (*54*), methemoglobin (*55*), and cytochrome P-450cam (*56*) also support this model.

The model proposed by Salemme predicts that the cyt b_5−cyt *c* complex is stabilized by electrostatic interactions between Glu44 and Lys27, Glu48 and Lys13, Asp60 and Tml72 (Tml, trimethyllysine), and heme propionate and Lys79 (cyt b_5 residues listed first) (*5*, *6*). In a second model complex, proposed by Mauk and co-workers (*7*), salt bridges are predicted to form between Glu56 and Lys87, Glu48 and Arg13, Asp60 and Lys86, and heme propionate and Tml72 (cyt b_5 residues listed first). Our combined data currently cannot distinguish between these two slightly different models. The relaxation and cross-saturation experiments indicate that there is no direct involvement of the second, cleft, region of cyt b_5 in the binding process. The chemical shift perturbations observed in the cleft site in this study and a previous study (*10*) are thus most likely due to indirect effects. These may include subtle conformational adaptations of this rather flexible area (*9*) in a changed electrostatic potential caused by formation of the complex.

SUMMARY

The association between ferrous cyt b_5 and ferrous cyt *c* occurs in a 1:1 stoichiometry. The binding is relatively weak

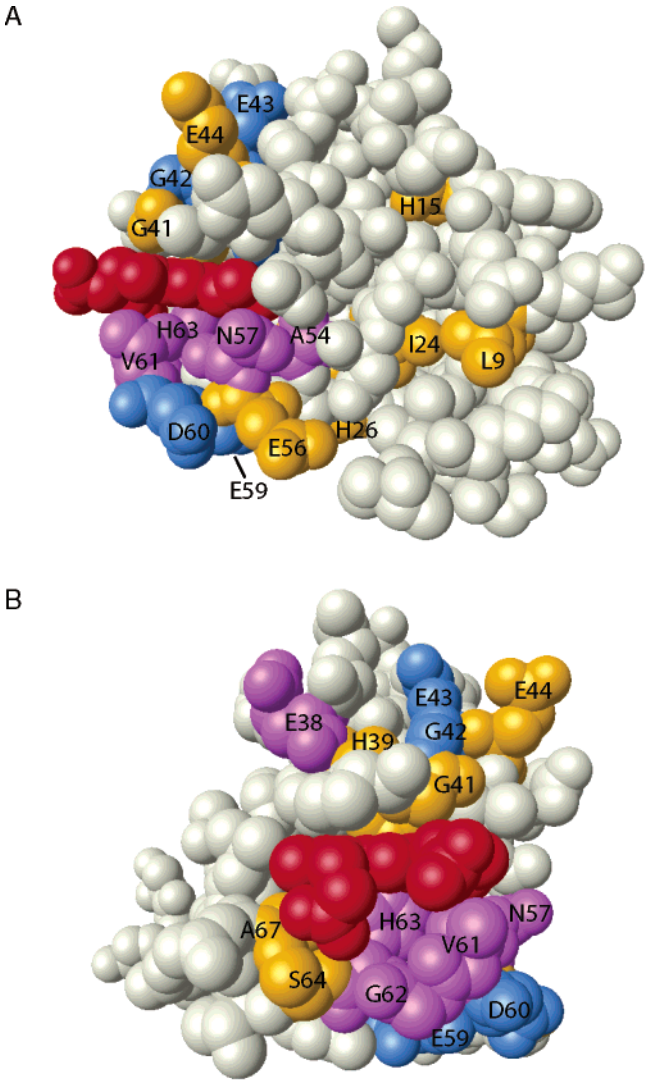

FIGURE 9: Summary of NMR data mapped onto a space-filling model of bovine cyt b_5. (A) The residues that exhibit a significant change in peak height in the cross-saturation experiment are colored blue. The heme is colored red. (B) A 90° rotation of panel A (PDB entry 1cyo) (*57*). This figure was made using MOLMOL (*34*). The residues that exhibit a change in dynamic behavior are colored purple, and the residues which undergo a chemical shift greater than the average change in chemical shift plus one standard deviation are colored yellow.

with an apparent K_a of $(6 \pm 3) \times 10^4$ M^{-1} and exhibits a dissociation rate constant with a lower limit of 180 s^{-1}. Chemical shift mapping experiments, combined with ^{15}N relaxation and saturation transfer experiments, were used in combination to identify the residues of cyt b_5 involved in the binding interface. The complex between cyt b_5 and cyt c is found to exist predominantly in an orientation in which the negatively charged surface around the exposed heme edge of cyt b_5 creates the binding interface for cyt c recognition, corroborating the models proposed by Salemme (*5*, *6*) and Mauk (*7*). Further studies must be performed to distinguish between these slightly different models and to identify the complementary binding face on cyt c before we can have a complete structural understanding of this weakly associated electron transfer complex.

ACKNOWLEDGMENT

Dr. Shawn Y. Stevens is most gratefully acknowledged for the saturation transfer experiments and involvement with the writing of the manuscript. The W. M. Keck Foundation is acknowledged for support of the purchase of the 800 and 500 MHz spectrometers. We are grateful to Carol Chanter for help in preparing the manuscript for publication.

REFERENCES

1. Mauk, M. R., Reid, L. S., and Mauk, A. G. (1982) Spectrophotometric analysis of the interaction between cytochrome b5 and cytochrome c, *Biochemistry 21*, 1843−1846.
2. Banci, L., Bertini, I., Felli, I., Krippahl, L., Kubicek, K., Moura, J., and Rosato, A. (2003) A further investigation of the cytochrome b_5-cytochrome c complex, *J. Biol. Inorg. Chem. 8*, 777−786.
3. Whitford, D., Concar, D. W., Veitch, N. C., and Williams, R. J. P. (1990) The formation of protein complexes between ferricytochrome b_5 and ferricytochrome c studied using high-resolution ^{1}H-NMR spectroscopy, *Eur. J. Biochem. 192*, 715−721.
4. Mauk, A. G., Mauk, M. R., Moore, G. R., and Northrup, S. H. (1995) Experimental and theoretical analysis of the interaction between cytochrome c and cytochrome b_5, *J. Bioenerg. Biomembr. 27*, 311−330.
5. Salemme, F. R. (1976) An hypothetical structure for an intermolecular electron transfer complex of cytochromes c and b_5, *J. Mol. Biol. 102*, 563−568.
6. Wendoloski, J. J., Matthew, J. B., Weber, P. C., and Salemme, F. R. (1987) Molecular dynamics of a cytochrome c-cytochrome b_5 electron transfer complex, *Science 238*, 794−797.
7. Northrup, S. H., Thomasson, K. A., Miller, C. M., Barker, P. D., Eltis, L. D., Guillemette, G., Inglis, S. C., and Mauk, A. G. (1993) Effects of charged amino acid mutations on the bimolecular kinetics of reduction of yeast iso-1-ferricytochrome c by bovine ferrocytochrome b_5, *Biochemistry 32*, 6613−6623.
8. Rodgers, K. K., and Sligar, S. G. (1991) Mapping electrostatic interactions in macromolecular associations, *J. Mol. Biol. 221*, 1453−1460.
9. Storch, E. M., and Daggett, V. (1995) Molecular dynamics simulation of cytochrome b_5: Implications for protein−protein recognition, *Biochemistry 34*, 9682−9693.
10. Hom, K., Ma, Q.-F., Wolfe, G., Zhang, H., Storch, E. M., Daggett, V., Basus, V. J., and Waskell, L. (2000) NMR studies of the association of cytochrome b_5 with cytochrome c, *Biochemistry 39*, 14025−14039.
11. Ubbink, M., and Bendall, D. S. (1997) Complex of plastocyanin and cytochrome c characterized by NMR chemical shift analysis, *Biochemistry 36*, 6326−6335.
12. Veitch, N. C., Whitford, D., and Williams, R. J. P. (1990) An analysis of pseudocontact shifts and their relationship to structural features of the redox states of cytochrome b_5, *FEBS Lett. 269*, 297−304.
13. Worrall, J. A. R., Liu, Y., Crowley, P. B., Nocek, J. M., Hoffman, B. M., and Ubbink, M. (2002) Myoglobin and cytochrome b_5: A nuclear magnetic resonance study of a highly dynamic protein complex, *Biochemistry 41*, 11721−11730.
14. Rodríguez-Marañón, M. J., Qiu, F., Stark, R. E., White, S. P., Zhang, X., Foundling, S. I., Rodríguez, V., Schilling, C. L., III, Bunce, R. A., and Rivera, M. (1996) ^{13}C NMR spectroscopic and X-ray crystallographic study of the role played by mitochondrial cytochrome b_5 heme propionates in the electrostatic binding to cytochrome c, *Biochemistry 35*, 16378−16390.
15. Moore, G. R., Cox, M. C., Crowe, D., Osborne, M. J., Rosell, F. I., Bujons, J., Barker, P. D., Mauk, M. R., and Mauk, A. G. (1998) N-ϵ-Dimethyl-lysine cytochrome c as an NMR probe for lysine involvement in protein−protein complex formation, *Biochem. J. 332*, 439−448.
16. Garrett, D. S., Seok, Y. J., Peterkofsky, A., Clore, G. M., and Gronenborn, A. M. (1997) Identification by NMR of the Binding Surface for the Histidine-Containing Phosphocarrier Protein HPr on the N-Terminal Domain of Enzyme I of the *Escherichia coli* Phosphotransferase System, *Biochemistry 36*, 4393−4398.
17. Guiles, R. D., Siddhartha, S., DiGate, R. J., Banville, D., Basus, V. J., Kuntz, I. D., and Waskell, L. (1996) Pseudocontact shifts used in the restraint of the solution structures of electron transfer complexes, *Nat. Struct. Biol. 3*, 333−339.

18. Grzesiek, S., Bax, A., Clore, G. M., Gronenborn, A. M., Hu, J. S., Kaufmann, J., Palmer, I., Stahl, S. J., and Wingfield, P. T. (1996) The solution structure of HIV-1 Nef reveals an unexpected fold and permits delineation of the binding surface for the SH3 domain of Hck tyrosine protein kinase, *Nat. Struct. Biol. 3*, 340−345.
19. Shuker, S. B., Hajduk, P. J., Meadows, R. P., and Fesik, S. W. (1996) Discovering high-affinity ligands for proteins: SAR by NMR, *Science 274*, 1531−1534.
20. McKay, R. T., Tripet, B. R., Hodges, R. S., and Sykes, B. D. (1997) Interaction of the Second Binding Region of Troponin I with the Regulatory Domain of Skeletal Muscle Troponin C as Determined by NMR Spectroscopy, *J. Biol. Chem. 272*, 28494−28500.
21. Zuiderweg, E. R. P. (2002) Mapping protein−protein interactions in solution by NMR spectroscopy, *Biochemistry 41*, 1−7.
22. Ozols, J., and Strittmatter, P. (1964) The interaction of porphyrins and metalloporphyrins with apocytochrome b_5, *J. Biol. Chem. 239*, 1018−1023.
23. Margoliash, E., and Frohwirt, N. (1959) Spectrum of horse-heart cytochrome c, *Biochem. J. 71*, 570−572.
24. Grzesiek, S., and Bax, A. (1993) The importance of not saturating water in protein NMR. Application to sensitivity enhancement and NOE measurements, *J. Am. Chem. Soc. 115*, 12593−12594.
25. Cavanagh, J., Fairbrother, W. J., Palmer, A. G., and Skelton, N. J. (1996) in *Protein NMR Spectroscopy*, Academic Press, San Diego.
26. Fischer, M. W. F., Majumdar, A., and Zuiderweg, E. R. P. (1998*)* Protein NMR relaxation: theory, applications and outlook, *Prog. Nucl. Magn. Reson. Spectrosc. 33*, 207−272.
27. Stevens, S. Y., Sanker, S., Kent, C., and Zuiderweg, E. R. P. (2001) Delineation of the allosteric mechanism of a cytidylyltransferase exhibiting negative cooperativity, *Nat. Struct. Biol. 8*, 947−952.
28. Pang, Y., Buck, M., and Zuiderweg, E. R. P. (2002) Backbone dynamics of the ribonuclease binase active site area using multinuclear (^{15}N and ^{13}CO) NMR relaxation and computational molecular dynamics, *Biochemistry 41*, 2655−2666.
29. Nakanishi, T., Miyazawa, M., Sakakura, M., Terasawa, H., Takahashi, H., and Shimada, I. (2002) Determination of the interface of a large protein complex by transferred cross-saturation measurements, *J. Mol. Biol. 318*, 245−249.
30. Freeman, R., and Kupce, E. (1997) Decoupling: theory and practice. I. Current methods and recent concepts, *NMR Biomed. 10*, 372−380.
31. Delaglio, F., Grzesiek, S., Vuister, G. W., Zhu, G., Pfeifer, J., and Bax, A. (1995) NMRPipe: a multidimensional spectral processing system based on UNIX pipes, *J. Biomol. NMR 6*, 277−293.
32. Johnson, B. A., and Blevins, R. A. (1993) A computer program for the visualization and analysis of NMR data, *J. Biomol. NMR 4*, 603−614.
33. Bartels, C., Xia, T., Billeter, M., Guntert, P., and Wuthrich, K. (1995) The program XEASY for computer-supported NMR spectral analysis of biological macromolecules, *J. Biomol. NMR 6*, 1−10.
34. Koradi, R., Billeter, M., and Wüthrich, K. (1996) MOLMOL: a program for display and analysis of macromolecular structures, *J. Mol. Graphics 14*, 52−55.
35. Williamson, M. P., Asakura, T., Nakamura, E., and Demura, M. (1992) A method for the calculation of protein alpha-CH chemical shifts, *J. Biomol. NMR*, *2*, 83−98.
36. Haigh, C. W., and Mallion, R. B. (1972) New tables of "ring current" shielding in proton magnetic resonance, *Org. Magn. Reson. 4*, 203−228.
37. Ösapay, K., and Case, D. A. (1991) A new analysis of proton chemical shifts in proteins, *J. Am. Chem. Soc. 113*, 9436−9444.
38. Dangi, B., Sarma, S., Yan, C., Banville, D. L., and Guiles, R. D. (1998) The Origin of Differences in the Physical Properties of the Equilibrium Forms of Cytochrome b_5 Revealed through High-Resolution NMR Structures and Backbone Dynamic Analyses, *Biochemistry 37*, 8289−8302.
39. Guiles, R. D., Altman, J., Kuntz, I. D., and Waskell, L. (1990) Structural studies of cytochrome b_5: complete sequence-specific resonance assignments for the trypsin-solubilized microsomal ferrocytochrome b_5 obtained from pig and calf, *Biochemistry 29*, 1276−1289.
40. Qian, C., Yao, Y., Ye, K., Wang, J., Tang, W., Wang, Y., Wang, W., Lu, J., Wie, Y., and Huang, Z. (2001) Effects of charged amino-acid mutation on the solution structure of cytochrome b_5 and binding between cytochrome b_5 and cytochrome *c*, *Protein Sci. 10*, 2451−2459.
41. Eley, C. G. S., and Moore, G. R. (1983) ^{1}H-NMR investigation of the interaction between cytochrome *c* and cytochrome b_5, *Biochem. J. 215*, 11−21.
42. Cross, K. J., and Wright, P. E. (1985) Calibration of ring-current models for the heme ring, *J. Magn. Reson. 64*, 220−231.
43. Liang, Z.-X., Jiang, M., Ning, Q., and Hoffman, B. M. (2002) Dynamic docking and electron transfer between myoglobin and cytochrome b_5, *J. Biol. Inorg. Chem. 7*, 580−588.
44. Liang, Z.-X., Nocek, J. M., Huang, K., Hayes, R. T., Kurnikov, I. V., Beratan, D. N., and Hoffman, B. M. (2002) Dynamic docking and electron transfer between Zn-myglobin and cytochrome b_5, *J. Am. Chem. Soc. 124*, 6849−6859.
45. Burch, A. M., Rigby, S. E., Funk, W. D., MacGillivray, R. T., Mauk, M. R., Mauk, A. G., and Moore, G. R. (1990) NMR characterization of surface interactions in the cytochrome b_5-cytochrome c complex, *Science 247*, 831−833.
46. Crowley, P. B., Vintonenko, N., Bullerjahn, G. S., and Ubbink, M. (2002) Plastocyanin-cytochrome *f* interactions: The influence of hydrophobic patch mutations studied by NMR spectroscopy, *Biochemistry 41*, 15698−15705.
47. Mauk, M. R., Barker, P. D., and Mauk, A. G. (1991) Proton linkage of complex formation between cytochrome c and cytochrome b_5: Electrostatic consequences of protein−protein interactions, *Biochemistry 30*, 9873−9881.
48. Feher, V. A., and Cavanagh, J. (1999) Millisecond-timescale motions contribute to the function of the bacterial response regulator protein Spo0F, *Nature 400*, 289−293.
49. Wyss, D. F., Dayie, K. T., and Wagner, G. (1997) Two-state allosteric behavior in a single-domain signaling protein, *Protein Sci. 6*, 534−542.
50. Abbott, M. B., Dvoretsky, A., Gaponenko, V., and Rosevear, P. R. (2000) Modulation of cardiac troponin C-cardiac troponin I regulatory interactions by the amino-terminus of cardiac troponin I, *FEBS Lett. 469*, 168−172.
51. Volkman, B. F., Lipson, D., Wemmer, D. E., and Kern, D. (2001) Two-state allosteric behavior in a single-domain signaling protein, *Science 291*, 2429−2433.
52. Kami, K., Takeya, R., Sumimoto, H., and Kohda, D. (2002) Diverse recognition of non-PxxP peptide ligands by the SH3 domains from p67phox, Grb2 and Pex13p, *EMBO J. 21*, 4268−4276.
53. Takahashi, H., Nakanishi, T., Kami, K., Arata, Y., and Shimada, I. (2000) A novel NMR method for determining the interfaces of large protein−protein complexes, *Nat. Struct. Biol. 7*, 220−223.
54. Livingston, D. J., McLachlan, S. J., La Mar, G. N., and Brown, W. D. (1985) Myoglobin:cytochrome b_5 interactions and the kinetic mechanism of metmyoglobin reductase, *J. Biol. Chem. 260*, 15699−15707.
55. Poulos, T. L., and Mauk, A. G. (1983) Models for the complexes formed between cytochrome b_5 and the subunits of methemoglobin, *J. Biol. Chem. 258*, 7369−7373.
56. Stayton, P. S., Poulos, T. L., and Sligar, S. G. (1989) Putidaredoxin competitively inhibits cytochrome b_5-cytochrome P-450cam association: a proposed molecular model for a cytochrome P-450cam electron-transfer complex, *Biochemistry 28*, 8201−8205.
57. Durley, R. C. E., and Mathews, F. S. (1996) Refinement and structural analysis of bovine cytochrome b_5 at 1.5 Å resolution, *Acta Crystallogr. D52*, 65−76.

BI030145T